J Mater Sci (2007) 42:8957–8965
DOI 10.1007/s10853-007-1653-3

The micro-structural strain response of tendon

Vinton W. T. Cheng · Hazel R. C. Screen

Received: 13 December 2006 / Accepted: 1 March 2007 / Published online: 19 July 2007

Abstract Tendons are multi-level fibre-reinforced composites, designed to transmit muscle forces to the skeleton. During physiological loading, tendons experience tensile loads, which are transmitted through the structure to the cells, where they may initiate mechanotransduction pathways. The current study examines the structural reorganisation and resulting local strain fields within the tendon matrix under tensile load. It uses confocal microscopy to photobleached a grid onto the collagen and image its deformation under the application of incremental tensile strain. Six parameters are used to quantify fibril and fibre movement and examine the mechanisms of extension employed by fascicles.

Results demonstrated an inhomogeneous strain response throughout the matrix and large variability between samples. Local strains in the loading axis were significantly smaller than the applied values. However, large compressive strains, perpendicular to the loading axis, were recorded. The average Poisson's ratio (0.8) suggested cells may experience significant compression during loading. Deflection of the grid lines, indicating sliding between collagen fibres, and rotation of the grid were also recorded. These data highlight the non-homogenous strain environment of fascicles and provide further evidence for fibre sliding under tensile load. They also suggested a rotary component to tendon response, which may indicate a helical organisation to the tendon matrix.

V. W. T. Cheng · H. R. C. Screen (✉)
Medical Engineering Division, Department of Engineering,
Queen Mary, University of London, Mile End Road,
London E1 4NS, UK
e-mail: H.R.C.Screen@qmul.ac.uk

V. W. T. Cheng · H. R. C. Screen
IRC in Biomedical Materials, Department of Engineering,
Queen Mary, University of London, Mile End Road,
London E1 4NS, UK

Introduction

Tendons are fibrous connective tissues, specialised in the function of uniaxial, tensile force transmission [1]. Structurally, tendons are natural, multi-level fibre-reinforced composites, built from the basic collagen molecule into units of increasing diameter [2, 3]. The fibres are predominantly collagen type I, comprising between 70% and 90% of the tendon dry mass, depending on the location and functional role of the tendon within the body and the species of test subject [4, 5]. The collagen units are generally aligned in the direction of loading and are the principle load-bearing components of tendon, conferring much of its mechanical strength [6]. At the molecular level, individual tropocollagen molecules, approximately 280 nm in length, are packed at repeating 64 nm intervals to form microfibrils, which aggregate into fibrils [7, 8]. Structural integrity of the fibril is ensured by inter-molecular and inter-microfibrillar cross-links, which aid strain transfer between the discontinuous collagen molecules [9, 10].

The fibrils aggregate within the proteoglycan rich non-collagenous matrix to build fibres and fascicles, the higher order structural levels of the tendon. However, the detailed organisation of these levels and the mechanisms by which they facilitate the transfer of tensile load are less clearly characterised. A number of studies have attempted to determine the length and continuity of the collagen fibrils, although their large aspect ratio and imaging limitations have precluded a conclusive answer. Scanning electron

microscopy images, showing very few fibril ends in mature tissue, have led some authors to conclude that the fibrils are continuous throughout the length of the tendon [11]. However, analysis of the composition and arrangement of the non-collagenous matrix between fibrils, and an examination local mechanical properties have led other authors to hypothesise a model with discontinuous fibrils embedded within a functional non-collagenous matrix that directly facilitates strain transfer [12–14].

Electron microscopy studies have located the proteoglycan decorin, bridging adjacent collagen fibrils within tendon [15]. This has led to the development of a 'shape molecule' hypothesis, in which decorin is responsible for controlling shear resistance and maintaining structural integrity between adjacent discontinuous fibrils [16]. Decorin has a horseshoe shaped core protein that binds around collagen fibrils and a single, orthogonally aligned dermatan sulphate glycosaminoglycan (GAG) chain which bridges adjacent fibrils [13, 17]. It is hypothesised that the recruitment of a large number of weak van der Waals interactions between dermatan sulphate chains can provide sufficient shear resistance to control strain transfer between fibrils [16, 18].

X-ray diffraction studies also support the discontinuous fibril hypothesis, reporting that only 40% of the total strain applied to a tendon fascicle can be accounted for by fibril extension, indicating the remaining 60% must occur through relative movement between the higher structural levels [19, 20]. In agreement, confocal microscopy studies implicate fibre sliding as a dominant extension mechanism for tendon and other hierarchical collagenous materials [14, 21]. Using the tenocyte cell nuclei as markers of fibre motion, relative sliding of adjacent fibres has been visualised under the application of tensile load. In addition, further studies have demonstrated that altering the composition of the non-collagenous proteoglycan matrix influences the relationships between fibril and fibre sliding within tendon fascicles, supporting a possible role for proteoglycans in regulating strain transfer mechanisms [22]. These studies provide important data relating to cellular deformation and mechanotransduction; however the relationships between the cells and the collagen matrix will influence the observed response. In order to examine the matrix response directly, a recent study has utilised a fluorescent photobleaching technique to image the movement of the collagen fibrils themselves and examine the strain response of the tissue [23]. The authors photobleached lines through the collagen matrix prior to the application of tensile strain. From images of the lines under strain, they have suggested that fibril sliding dominates extension, shielding the tenocytes from excessive shear strains.

Fluorescent microscopy exploits the ability to visualise fluorophores by exciting them with laser light. By controlling the binding of fluorophores to particular molecules within a sample, specific structures can be visualised. Photobleaching techniques, which further utilise this principle, have gained considerable popularity in recent years, with the development of techniques such as fluorescent recovery after photobleaching (FRAP) and fluorescent loss in photobleaching (FLIP) for the analysis of cell dynamics [24]. In typical experiments a fluorescent labelled protein is incorporated into a sample and small target regions of the dye then photobleached by repeated exposure to high intensity light from a laser beam. At high intensities, the fluorophores are over excited causing them to permanently lose their ability to fluoresce. If the sample is then excited by a lower intensity laser, the undamaged fluorophores in the non-photobleached areas, will still fluoresce clearly demarcating the two regions. The mobility of cellular components can be examined through monitoring the movement of the remaining fluorescing fluorophores [25]. Although most commonly utilised to image cellular structures, it is possible to use photobleached lines as markers of strain within tissue samples, by staining the complete tissue matrix with a fluorescent dye and then selectively photobleaching regions to providing well controlled areas of the sample that will not fluoresce when the fluorophores are excited. The current study utilises this technique to examine strain transfer through tendon fascicles, testing the hypothesis that sliding will occur at both the fibril and fibre levels of the tendon hierarchy.

Materials and methods

For all experiments, fascicles were taken from the proximal end of the tails of male Wistar rats aged between 4 and 8 months. Fascicles, approximately 300 μm in diameter, were teased from the tails within five hours of sacrifice, cut to lengths of around 45 mm, and maintained in a moistened state, in paper towel soaked with phosphate buffered saline (PBS; Sigma, Poole, UK).

Straining system

Testing utilised a custom designed tensile straining rig (Fig. 1), able to load fascicles while in situ on the stage of a confocal microscope (TCS SP2, Leica Microsystems GmbH, Wetzlar, Germany). A series of preliminary tests were carried out to validate the system for the testing of tendon fascicles and to determine the loading environment.

The rig and the grips are made from stainless steel, to minimise corrosion and facilitate ease of cleaning and sterilisation. The grips are shaped as triangular wedges (Fig. 1b) in order to hold the fascicle adjacent to the glass coverslip against the base of the rig, enabling the objective

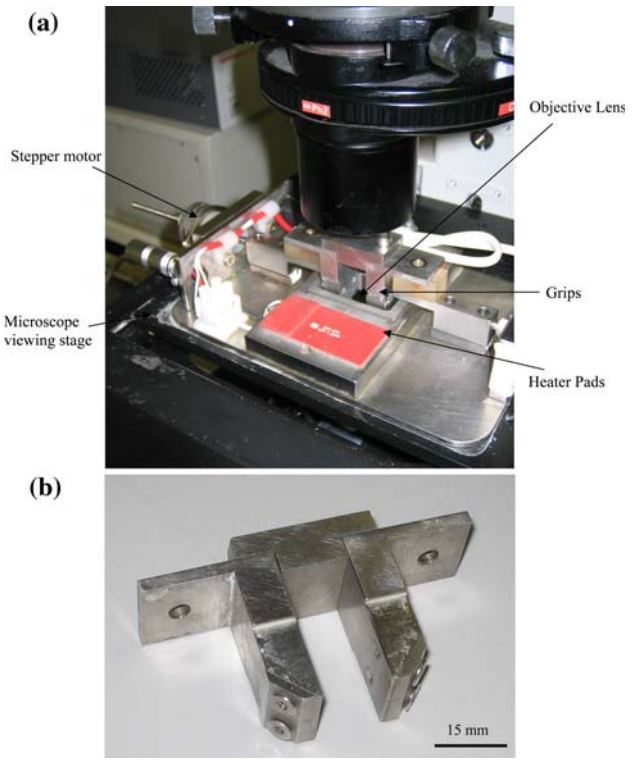

Fig. 1 Photographs of (**a**) the confocal rig on the microscope stage and (**b**) the grips for straining the sample

lens to focus internally within the tissue. Grips are maintained in horizontal alignment by a ball slider attached to the lid of the rig, and stepping linear actuators control the movement of the grips, allowing accurate and reproducible strains to be applied to the specimen. Each step is 25 ± 5 μm, corresponding to a strain of less than 0.02% on a sample of length 15 mm. The maximal uniaxial displacement is 15 mm, and the motors can withstand loads of up to 50 N.

Fifteen incremental strain to failure tests were carried out within the rig. Fascicles were secured in one grip and allowed to hang under their own weight while the second grip was positioned and then tightened, creating a test length of 15 mm and defining the 0% strain position. The grips were then loaded into the rig, immersed in PBS, and the rig placed on the stage of the confocal microscope, enabling the sample to be imaged under standard brightfield light microscopy using a 4× magnification objective lens (Plan Apo x4, Nikon, Kingston-Upon-Thames, UK). The fascicles were loaded to failure in 1% strain increments at a strain rate of 10% min^{-1}, taking an immediate snap shot of the grips and sample at each increment. From these images, the displacement of the grips at each increment was examined and compared with the specified applied displacement. In addition, the fascicles were examined after failure, to assess the location and mechanism of failure.

A further ten fascicles were subjected to a second series of validation experiments. Samples were secured in the rig in the same manner, and imaged under brightfield settings using a 10× magnification air immersion objective lens (Plan Apo x10, Nikon, Kingston-Upon-Thames, UK). Fascicles were once again loaded to failure in 1% strain increments at a rate of 10%/min^{-1}, with a hold time of approximately 20 s at each increment, while an image of the sample was recorded from which the gross sample and collagen fibre orientation was examined. Once again, the mechanism and location of failure was determined for each fascicle.

Microstrain analysis

In order to examine the microstrain environment, twenty fascicles were subjected to a sequential incubation in viable fluorescent dyes to stain the collagen and the cell nuclei. Each sample was incubated at room temperature (24 °C) following the procedure outlined below:

1. Twenty minutes (20 min) in 5-dicholorotriazynl fluorescein (5-DTAF; Molecular Probes, Oregon, USA) at a concentration of 2 mg/mL 0.1 M sodium bicarbonate buffer (pH 9; Sigma, Poole, UK) to stain the collagen components.
2. Twenty minutes (20 min) post-staining wash in PBS.
3. Forty minutes (40 min) in 5 mM Acridine orange (Sigma, Poole, UK) in PBS to stain the tenocyte nuclei.

Specimens were then briefly rinsed in PBS, prior to loading into the confocal straining rig at a test length of 15 mm, following the procedure described in the ''Straining system'' section. The orientation of each sample was checked under brightfield settings, with a 20× magnification air immersion objective lens (HC PL Fluotar, Nikon, Kingston-Upon-Thames, UK) and the fascicle then photobleached, using a 488 nm Krypton-Argon laser. A series of 1 μm thick lines were bleached in the central region, through the full width of the 5-DTAF stain, to create a grid of four identical squares, 50 μm × 50 μm. The laser intensity was then reduced to the imaging range, and the sample imaged with the same objective lens at a resolution of 2,048 × 2,048 pixels.

An image of the photobleached grid was taken in a focal plane approximately 20–25 μm from the sample surface, identified by the cell nuclei. The fascicle was then strained to 1% at a rate of 10%/min^{-1} and the cell nuclei used to refocus the grid at the same focal depth, before imaging again. Each fascicle was loaded to 2%, 4%, 6% and 8% strain, and the grid imaged at each strain increment, with a hold period of approximately 45 s before imaging at each increment, whilst the focal plane was located. In addition, a

series of ten images were taken at 15 μm increments through the thickness of the sample, at the 8% applied strain increment.

Image analysis

Images were processed using the analysis software Image J (1.34s, National Institute of Health, USA) following a similar procedure to that previously described by Bruehlmann and co-workers [23]. Two identical copies of each image were filtered using Gaussian blur filters with radii of 10 and 20 pixels. The images were subtracted before thresholding and skeletonising, to produce a single pixel trace of the photobleached grid following the midline of the original conformation (Fig. 2a). Any dirt or noise not related to the photobleached region was removed, and the pixel co-ordinates for the grid converted to data points for analysis in Excel (Excel 2003, Microsoft Corp., Redmond, WA).

Six parameters, shown in Fig. 2b, were qualitatively analysed to describe the in situ micromechanical environment.

- x strain ($100\Delta x/x$) Percentage strain in x direction (with axis of loading)
- y strain ($100\Delta y/y$) Percentage strain in y direction (perpendicular to loading axis)
- y angle (θ_y) Angle of perpendicular lines relative to the y direction
- x angle (θ_x) Angle of parallel lines relative to the x direction
- Deflection (d) Step deflection along the length of the y line
- Displacement (D) Displacement between ends of y line along the x axis

Statistical analysis

Each parameter was analysed for the effect of increasing strain application using StatsDirect (2005, StatsDirect Ltd., Cheshire). Analysis of Variance (ANOVA) statistical tests and Tukey post-hoc tests for analysing multiple comparisons of mean were applied. Statistical significance was set at $p < 0.05$.

Results

Straining system

The grip displacement at each strain increment, measured from the 4× magnification brightfield images, closely followed that applied to the stepper motors, with a variability between predicted and measured displacement of ±5 μm (3.3%). The grips successfully held the individual fascicles and no slippage occurred in any of the samples. Twelve of the samples (80%) failed in the central region at a distance from each grip, and failure occurred through a slow unravelling of the collagen fibres.

Examination of the fascicles under 10× magnification brightfield light microscopy demonstrated that the samples were aligned in the grips, and that the collagen fibres were fully aligned in the direction of loading (Fig. 3). At the gross level that fascicle was loaded uniformally and maintained the same orientation throughout testing. The crimped fibres were seen to straighten and extend and no rotation was visible. Sample failure was visualised as a pull out of adjacent groups of fibres. Commencing at a strain increment between 9% and 13%, visible relaxation of the matrix became apparent, followed by sliding between groups of fibres at random locations across the sample width. The same sliding behaviour was visible along the length of the sample, and failure was finally seen to occur through complete pull out of adjacent fibre groups, occurring at the 14% increment in the majority (70%) of samples.

Microstrain results

A series of images from an example fascicle at 0%, 4% and 8% strain are shown in Fig. 4. Distortion of the photo-

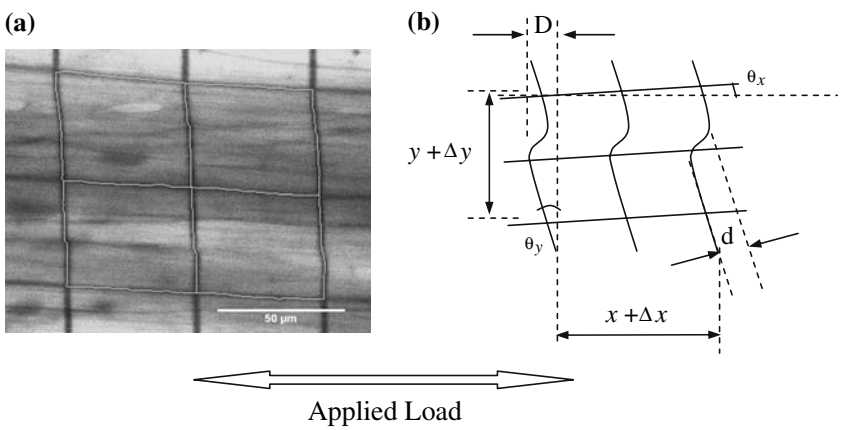

Fig. 2 (**a**) Typical confocal image of a photobleached grid at a depth of 30 μm into the fascicle and at 4% applied strain, showing the image processing to provide a single pixel trace of the grid. (**b**) Schematic of the grid after deformation, showing the six deformation measurements

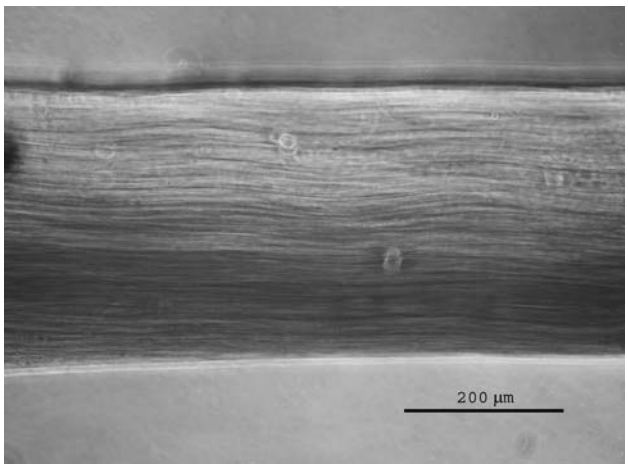

Fig. 3 Typical image of an unstrained fascicle under brightfield imaging, as taken at the start of every test. Image shows the alignment of the collagen fibres at the start of loading

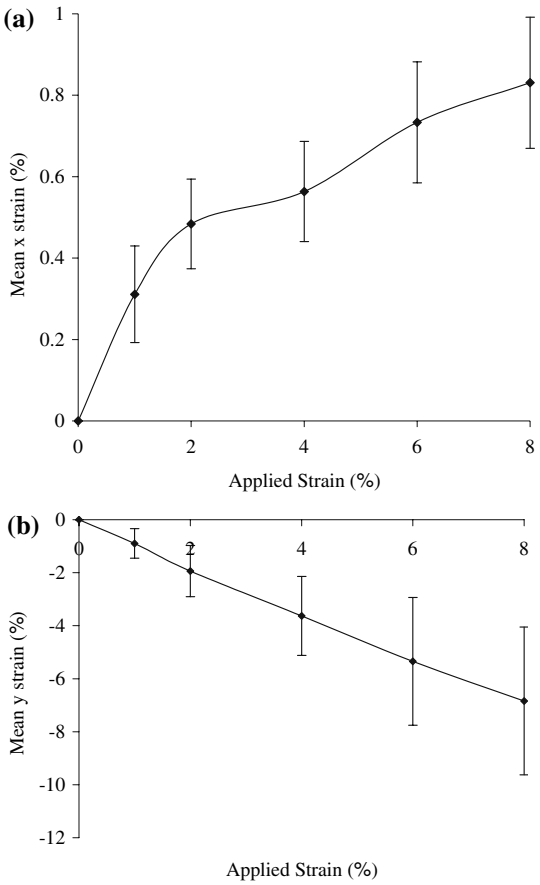

Fig. 5 Mean local strain curves showing how (**a**) the *x* strain (n = 20) and (**b**) the *y* strain (n = 11), in the grid change with applied strain. Data depicts mean and standard error

bleached grid was recorded in every sample, indicating an inhomogeneous response to strain within the fascicle. However, the nature of the strain response was highly variable between samples. Figure 5a plots the mean strain across the grid in the direction of loading (*x* strain) against the applied strain for each increment. The local *x* strain demonstrated a statistically significant increase during the initial 2% of applied load, equalling a quarter of the applied strain. With increasing applied strain, the rate of increase decreased, leading to a local strain approximately 10% of the applied value at 8%. The maximum local *x* strain recorded in any sample was 2.5%.

By contrast, the local *y* strains perpendicular to the loading axis (Fig. 5b) were highly variable, but indicated large compressive strains. There was a linear relationship between applied strain and mean *y* strain with a mean Poisson's ratio of 0.8 taken over all data points. Data from some fascicles indicated a Poisson's ratio in excess of 1, with compressive *y* strains reaching values greater than –10% at 8% applied strain.

The other four strain parameters analysed the degree and nature of distortion within the grid (Figs. 6, 7). Once again, the contribution of each parameter varied between samples, as summarised in Table 1. A point of deflection (*d*) was seen along the length of perpendicular grid lines, which increased with applied strain in a statistically significant manner. The deflection increased most rapidly during the initial 2% of straining (Fig. 6a) and was clearly visible to the eye (over 5 µm) in 55% of the samples, reaching a mean value of 5.8 µm at 8% applied strain. The deflection reached over 16 µm in two samples, accounting for approximately 2% of the applied displacement.

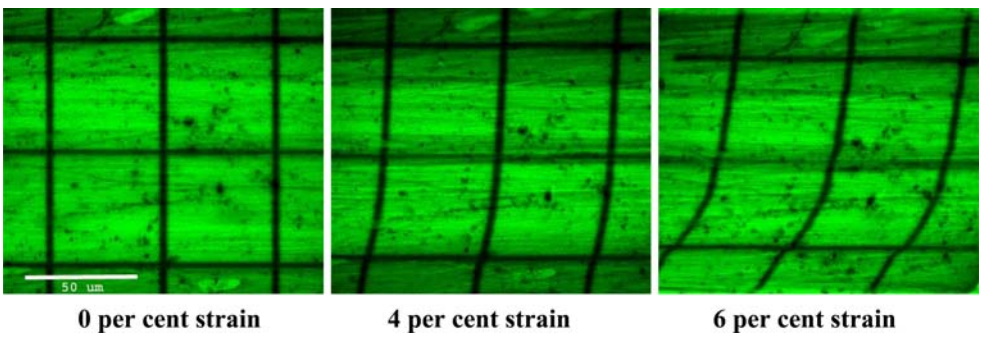

Fig. 4 Images of the strain grid in a typical sample at 0%, 4% and 8% applied strain

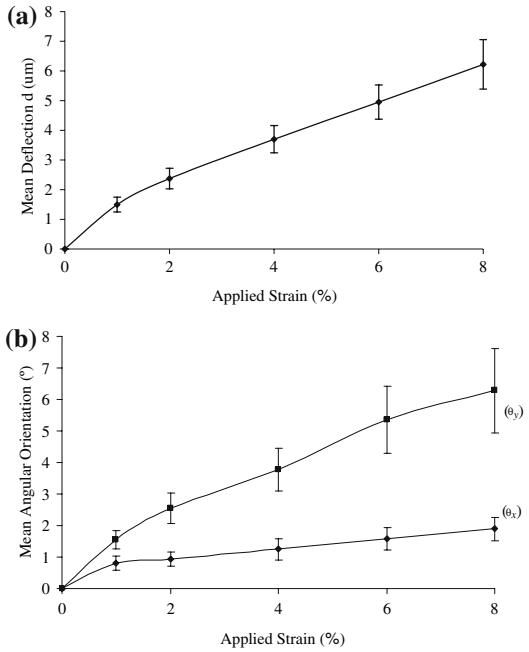

Fig. 6 Analysis of the mean local strain response of the grid with applied strain depicting (**a**) the size of step deflections (d) along the length of a line and (**b**) the angular reorientation of the lines. θ_y denotes the angle of the perpendicular lines, relative to the initial y direction and θ_x the angle of the parallel lines relative to the initial x direction. Data depicts mean and standard error. (d) $n = 20$; (θ_y) $n = 20$; (θ_x) $n = 11$

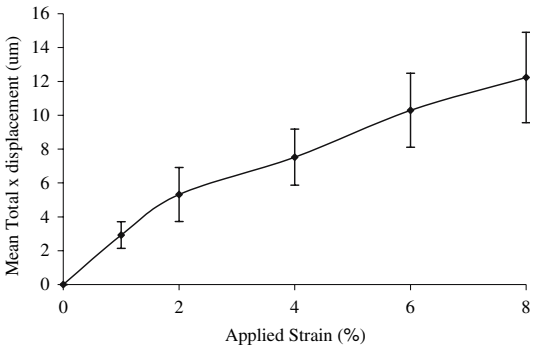

Fig. 7 Analysis of the total displacement (D) enabled across the length of the grid. Data depicts mean and standard error ($n = 20$)

The gridlines perpendicular to the loading axis demonstrated a rotation, relative to their original orientation (θ_y). Rotational direction varied between samples, hence absolute values are reported, in order to assess the extent of the reorientation. The reorientation θ_y demonstrated a statistically significant trend of increasing with applied strain to reach a mean absolute value of 6.2° (Fig. 6b).

The angular reorientation of the parallel grid lines (θ_x) followed the direction of θ_y for each individual fascicle but was consistently statistically smaller. The mean absolute angle followed a statistically significant trend of increasing with applied strain, to reach a mean value of 1.9° at 8% applied strain (Fig. 6b). However, the parallel lines became distorted in each sample as the fibres became fully aligned in the direction of loading, limiting the resolution capability of this measurement.

Displacement D provides a single measure to determine the total grid deformation in the parallel plane. As reported for other strain parameters in the perpendicular plane, the most rapid increase was seen during the initial 2% of applied strain, after which a continual linear increase was recorded to reach a mean maximum of 12.3 μm at 8% strain (Fig. 7). The 100 μm square grid covered approximately one third of the total fascicle width (~300 μm). As such, total displacement across the fascicle width may be in the range of 30–40 μm, accounting for approximately 3% of the applied displacement.

The analysis of the z-series images, taken at 8% applied strain, demonstrated a non-homogenous strain response through the thickness of the sample. The variation in local x and y strain with depth for three typical fascicles are shown in Fig. 8. The x strain was seen to vary by a mean amount of 0.3% through the thickness of each sample, compared with a mean of 2% for the y strain. Both variations are around a quarter of the mean local strain value for the parameter, reported in Fig. 6.

Discussion

The confocal rig used for the current study provides a mechanism of incrementally loading tendon fascicles in a controlled manner, whilst visualising their in situ micromechancial environment. Using the rat tail tendon model, direct staining and photobleaching of the collagen matrix was employed to provide a clear mechanism of monitoring collagen behaviour directly. Validation experiments confirmed a controlled loading environment, in which the fascicles were securely gripped and subjected to uniform loading at the gross level, enabling the sub-structural response to be examined.

The use of the two viable fluorescent dyes, 5-DTAF and Acridine Orange, enabled both the cells and the photobleached grid to be viewed simultaneously. The cells provided an important marker to ensure all images were taken at the same focal depth, and the ability to image the cells and grid at the same wavelength ensured a minimal imaging period at each increment. The suitability of both stains has been demonstrated in previous publications, with 5-DTAF successfully staining collagen fibres in vitro and in vivo [23, 26, 27], and Acridine Orange staining tenocyte nuclei [14, 28]. However, the two dyes are rarely used together, as they share similar absorption/emission maxima. Results demonstrated competitive staining between

Table 1 Summary of mean data and range of values recorded for each deformation parameter at the 8% applied load increment

Values at 8% applied strain	x strain (%)	y strain (%)	Deflection, d (μm)	Angle, θ_y (°)	Angle θ_x (°)	Displacement, D (μm)
Sample number	20	11	20	11	20	20
Minimum value	0.17	–0.48	0.73	1.05	0.84	1.7
Maximum	2.49	–11.16	16.05	15.3	3.35	35.6
Mean value	0.83	–6.84	6.22	6.2	1.9	12.3
Standard error	0.16	2.8	0.83	1.3	0.37	2.7

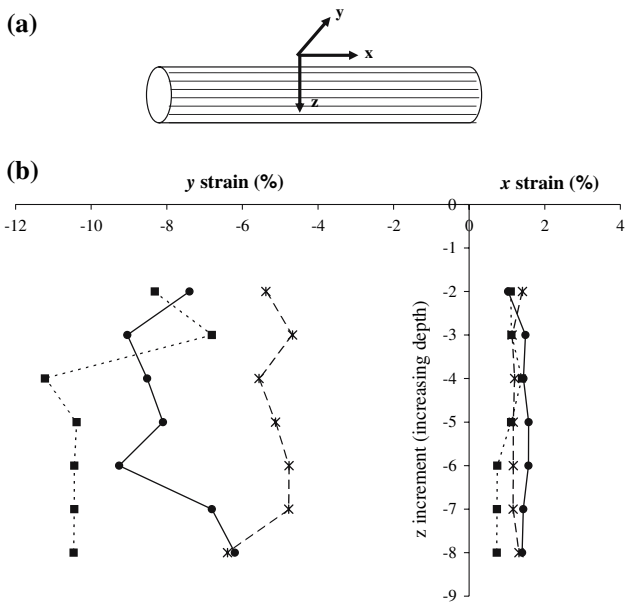

Fig. 8 (**a**) Image of a fascicle, denoting the orientation of the x, y and z planes. (**b**) The variation in x strain and y strain with depth through three typical fascicles, at 8% applied strain. Owing to the limited z-resolution, depth is given in arbitrary units, where 1 unit is approximately 15 μm

the two dyes, evident from the limited number of visible cells. As the cell density was insufficient to confidently ascertain the fibre boundaries, there was no attempt to establish where line deflections occurred in relation to the fibrillar structures. However, enough cells were visible to provide location markers for depth and ensure the grid was continually imaged in the same focal plane. The use of a 20× microscope objective lens greatly simplified tracking of the grid and provided a clear overview of the fascicle response. However, its low numerical aperture limited its depth correction capabilities in the z-plane to approximately 1.28 μm, compared with 0.68 μm in the x–y plane [29]. Data from z-series images were subsequently presented using arbitrary units and confined to providing an indication of the change in x–y parameters at each depth increment.

The staining procedures necessitate a period of incubation in solution to enable the uptake of dye. Previous studies by the authors have demonstrated a swelling of fascicles in response to incubation in different solutions, and a subsequent change in the local strain parameters [22]. It is not possible to carry out these analyses without an incubation step, and the fascicles in the current study have been treated in a similar fashion to the control (unswollen) fascicles in the previous work. The differences recorded between fascicles in the earlier work were attributed to the longer twenty-four hour incubation period, however, it should be noted that some swelling effects may be seen in all of the untreated fascicles, including those in the current study.

Monitoring deformation of the grid enabled the analysis of a series of local strain parameters, related directly to changes in the fibre or fibrillar structure. As in previous studies, there was a delay of approximately 60 s between straining the sample and taking the image, whilst the grid was located and the image focused in the correct focal plane. Recent studies by the authors have examined the stress relaxation response of tendon fascicles during the initial 60 s after loading (not currently published). These data have demonstrated that the majority of relaxation occurs during the initial 15 s of the relaxation period, by sliding between adjacent fibres. About 45 s after the load had been applied, the relaxation rate had significantly slowed, suggesting that in the current study, the fascicle response was analysed after stress relaxation effects.

In good agreement with previous studies, the local strain in the direction of loading was found to be significantly smaller than the applied strain at the fascicular level and the strain response non-homogenous across the fascicle width [14, 23]. The development of differential strain fields with the application of strain would be expected in such a non-heterogeneous structure, and has previously been attributed to the sequential straightening and loading of individual fibrils with different crimp periodicity [30]. This may also explain the variability seen in each parameter, with the deformation seen dependent on the crimp angle, the original orientation of the collagen fibres and the order in which they straighten, all of which will vary with imaging location.

Although the local x strain remained small, a progressive increase in the compressive y strain was recorded,

indicative of a reduction in fibre diameter as the fascicle was subjected to tensile loading (Fig. 5b). The mean Poisson's ratio, calculated to be 0.8, suggests that there may be significant compressive forces generated within the matrix under physiological loading conditions, that could be transmitted to the cells, influencing the mechanotransduction pathways. One possible explanation for the large Poisson's ratio is the exudation of fluid from the extracellular matrix during stretching, as previously reported [31, 32]. Electron microscopy has demonstrated interfibrillar space within the structure, which may well facilitate this response [22]. A visible improvement in the definition of the collagen fibrils with increasing strain was also noted, and images demonstrated fibrils falling in and out of the focal plane. Both of these factors may be associated with fibre alignment to the axis of loading and result in a reduction of interfibrillar space.

The compressive strains in the fascicle matrix are larger than those previously reported for compressive nucleus strains under tensile load [28]. However, previous cell mechanics studies have demonstrated that the nucleus of connective tissue cells is generally stiffer than the surrounding cytoplasm [33], hence strains may be representative of those experienced by the cell body. Compression of the tendon ultrastructure under tensile load has also been described by Wang and co-workers [34] using laser Raman spectroscopy to examine the response of rat tail tendon fascicles to uniaxial tension. The authors reported a rise in wavelength shift after the toe region of the loading curve, indicating lateral compression of the collagen fibre, possibly associated with the reorganization of the chemical groups (particularly carbonyls) aligned orthogonally to the axis of applied strain.

Deflection (d) was employed as a measure of relative sliding between collagen structures. Most samples demonstrated a single deflection across the width of the 100 μm grid, indicative of sliding behaviour at the fibre level. However, the limited capability to image cells meant it was not possible to confirm that this point of deflection was at a fibre edge. Deflections of up to 16 μm were seen in samples, with a mean value of 6.2 μm at 8% applied strain. This accounts for less than 1% of the applied displacement, however the grid covered approximately one third of the fascicle width, so further deflection sites may be present across the width. These values were smaller than those previously reported for sliding behaviour between rows of tenocytes [14, 22]. However, it is notable that the sliding values previously reported by Screen and co-workers closely match the maximum displacement measurement D taken in the current study. The displacement D incorporated both rotation and displacement of the grid and reached a mean maximum value of 12.2 μm at 8% applied strain. In previous studies, the analysis of nuclei position would not have been able to differentiate between these two parameters, hence the previous data may well have been ascribed to rotation as well as fibre sliding and may provide further explanation of why cells are seen to fall in and out of focus.

In the current study, rotation was measured independently, through an analysis of angular reorientation of grid lines, both perpendicular and parallel to the loading axis. Reorientation of perpendicular lines, reached a mean angle of 6.2° and coupled with reorientation and distortion of the parallel grid lines, indicates there may be a rotary element to the sample strain response, supporting the hypothesis of a helical tendon structure. Helical crimp patterns have previously been reported in tendon [35, 36]. Using interference and polarised light microscopy, de Campos Vidal [36] demonstrated wide variations in geometric features and birefringence in the crimp structure of bovine and rat tail tendon sections, which was attributed to a spiralling fibril arrangement and a helical supra-organisation. In addition, Kannus [37] described how fascicles, or tertiary tendon bundles, frequently showed a spiral formation along the course of the tendon. The chirality of the collagen molecule has led a number of authors to hypothesise a superstructure showing elements of ''handedness'', as a helical organisation would improve stability of higher order structures through reciprocity in winding patterns [38–40]. This has caused some controversy, with other authors suggesting that the reduced stiffness associated with a helical structure would be too inefficient for the tendon to effectively transfer force [41]. Although such a structure would imply a less efficient means of transferring muscle action to the skeleton, a helical organisation would be better suited to resist flexion, lateral compression or multidirectional deformation, all of which have been reported to occur within tendon [4].

This study has concentrated on extension mechanisms enabled by fibril and fibre movement within a single focal plane. However, as a three dimensional structure, it would be anticipated that similar extension mechanisms should be seen in the z-plane. The z-series of images taken at 8% applied strain confirmed that strain dispersal through the matrix incorporated relative sliding between fibres in the z-plane also. In agreement with data relating to individual x–y planes (Fig. 5), greater variation was recorded in the y strains. However, it was notable that the extent of the variability equated to approximately a quarter of the mean strain value for that parameter.

Sliding has been implicated in a number of micromechanical studies as a mechanism for strain transfer and the subsequent extension of tendon fascicles [14, 20, 21]. The current study provides further evidence of sliding behaviour within the tendon ultrastructure, but also indicates that rotation occurs in undamaged fascicular samples. It

indicated that tendon extension could be consistent with a helical or spiral geometry in the fascicular structure, whereby extension is facilitated by a straightening of the coil in addition to fibre sliding.

Acknowledgement Many thanks to Dr. Martin Knight, for his expert advice and assistance with the confocal microscopy.

References

1. Woo SLY (1982) Biorheology 19:385
2. Harris B (1980) Symp Soc Exp Biol 34:37
3. Hiltner A, Cassidy JJ, Baer E (1985) Ann Rev Mater Sci 15:455
4. Benjamin M, Ralphs JR (1997) Histol Histopathol 12:1135
5. Ker RF (2002) CBPA 133:987
6. Elliott DM, Robinson PS, Gimbel JA, Sarver JJ, Abboud JA, Iozzo RV, Soslowsky LJ (2003) Ann Biomed Eng 31:599
7. Wess TJ, Hammersley AP, Wess L, Miller A (1998) J Struct Biol 122:92
8. Buehler MJ (2006) PNAS 103(33):12285
9. Avery NC, Bailey AJ (2005) Scan J Med Sci Sports 15:231
10. Wess TJ, Cairns DE (2005) J Synchrotron Rad 12:751
11. Provenzano PP, Vanderby R Jr (2006) Matrix Biol 25:2–71
12. Derwin KA, Soslowsky LJ, Kimura JH, Plaas AH (2001) J Orthop Res 19:269
13. Redaelli A, Vesentini S, Soncini M, Vena P, Mantero S, Montevecchi FM (2003) J Biomech 36:1555
14. Screen HR, Lee DA, Bader DL, Shelton JC (2004) J Eng Med 218:109
15. Scott JE, Orford R (1981) Biochem J 197:573
16. Scott JE (2003) J Physiol 55:2–335
17. Weber IT, Harrison RW, Iozzo RV (1996) J Biol Chem 271:31767
18. Vesentini S, Redaelli A, Montevecchi FM (2005) J Biomech 38:433
19. Sasaki N, Odajima S (1996) J. Biomech 29(5):655
20. Puxkandl R, Zizak I, Paris O, Keckes J, Tesch W, Bernstorff S, Purslow P, Fratzl P (2002) Philos Trans R Soc Lond B Biol Sci 357:191
21. Bruehlmann SB, Matyas JR, Duncan NA (2004) Spine 29:2612
22. Screen HR, Shelton JC, Chhaya VH, Kayser MV, Bader DL, Lee DA (2005) Ann Biomed Eng 33(8):1090
23. Bruehlmann SB, Kelly EJ, Duncan NA (2005) Trans Orthop Res Soc 30:389
24. Goodwin JS, Kenworthy AK (2005) Methods 37:154
25. Koster M, Frahm T, Hauser H (2005) Curr Opin Biotech 16:28
26. Woo HM, Kim MS, Kweon OK, Kim DY, Nam TC, Kim JH (2001) Br J Ophthalmol 85:345
27. Davison PF, Galbavy EJ (1985) Invest Ophthalmol Vis Sci 26:1202
28. Arnoczky SP, Lavagnino M, Whallon JH, Hoonjan A (2002) J Orthop Res 20:29
29. Petrán M, Boyde A, Hadravsky M (1990) In: Confocal microscopy. Academic Press, London, vol 9, p 262
30. Hansen KA, Weiss JA, Barton JK (2002) J Biomech Eng 124:72
31. Lanir Y, Salant EL, Foux A (1988) Biorheology 25:591
32. Hannafin JA, Arnoczky SP (1994) J Orthop Res 12:350
33. Knight MM, van de Breevaart Bravenboor J, Lee DA, van Osch GJVM, Weinans H, Bader DL (2002) Biochim Biophys Acta 1570:1
34. Wang YN, Galiotis C, Bader DL (2000) J Biomech 33:483
35. Yahia LH, Drouin G (1989) J Orthop Res 7:2–243
36. de Campos Vidal B (2003) Micron 34:423
37. Kannus P (2000) Scand J Med Sci Sports 10:312
38. Ottani V, Martini D, Franchi M, Ruggeri A, Raspanti M (2002) Micron 33:587
39. Wess TJ, Hammersley AP, Wess L, Miller A (1998) J Mol Biol 275:255
40. de Campos Vidal B (2006) Matrix Biol 25:132
41. Raspanti M, Manelli A, Franchi M, Ruggeri A (2005) Matrix Biol 24:503